WILEY | Hindawi

Research Article

Investigation on Hydration and Deformation Characteristics of Shale Using X-ray Computed Tomography

Yong-Ting Duan [iD],[1,2] **Xiao Li,**[3,4] **Bo Zheng,**[3] **and Bai-Cun Yang** [iD][5]

[1]*Key Laboratory of Ministry of Education on Safe Mining of Deep Metal Mines, School of Resources and Civil Engineering, Northeastern University, Shenyang 110819, China*
[2]*Key Laboratory of Liaoning Province on Deep Engineering and Intelligent Technology, Northeastern University, Shenyang 110819, China*
[3]*Key Laboratory of Shale Gas and Geoengineering, Institute of Geology and Geophysics, Chinese Academy of Sciences, Beijing 100029, China*
[4]*Institutions of Earth Science, Chinese Academy of Sciences, Beijing 100029, China*
[5]*School of Resources and Civil Engineering, Northeastern University, Shenyang 110819, China*

Correspondence should be addressed to Yong-Ting Duan; duanyongting@mail.neu.edu.cn

The physical and mechanical properties of shale are significant for completion engineering and fracturing design for shale oil and gas production. To further study the water effect and the deformation characteristics of shale, some cylindrical specimens were soaked at three periods (0, 20, and 60 days), the in situ uniaxial compression tests were conducted, and the CT technique was used at different hydration and loading stages. Based on the CT results, the image gray variance value in each hydration specimen was extracted; the evolution results show that the water imbibition has a significant influence on the structure of shale in the early soaking stage, and the influence degree is more evident in the external region. Moreover, the water influence on the mechanical property of shale was analyzed by comparing the failure characteristics of specimens with and without hydration; the CT results show that the hydration treatment affects the failure mode of shale. In addition, a new method based on the CT image was proposed to calculate the lateral strain; the evolution of the axial stress-strain curve reveals that the expansion phenomena exist before failure, and the evolution process includes four stages. At last, the differences in the deformation degree were discussed by analyzing the volumetric strain at different CT scanning layers; the results reflect the expansion or compression degree along with the specimen height. Those conclusions can help us further understand the water effect and the deformation characteristics of shale oil and gas reservoirs.

1. Introduction

In 2018, China's dependency on foreign oil and natural gas had reached 69.8% and 45.3%. Exploring and developing complementary and replacement sources of conventional energy have become top priorities. Shale oil and gas, as unconventional energy, have attached attention and will play an essential role in ensuring China's oil and gas security and economic growth [1–3]. So far, hydraulic fracturing is a commonly used technique for recovery enhancement in shale oil and gas development. Shale's physical and mechan-

ical properties are of great significance for completion engineering and fracturing design for shale oil and gas production [4, 5].

Previous studies [6, 7] have shown that the fraction of recovered flow backwater with an average of 10% or less after fracturing operation, and water absorption in shale often causes the swelling of rocks, leading to cracks and fractures. In order to find out how the remaining fracturing fluid affects the shale formation, some experimental studies about the water effect on shale have been made. Ma and Chen [8] investigated the mesodamage characteristics of shale

(a)   (b)
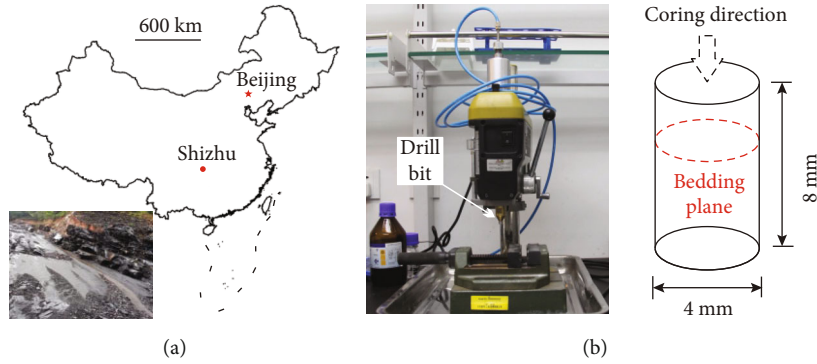
FIGURE 1: The location of sampling (a), the hand-operated electric drill and the diagram of a specimen (b).
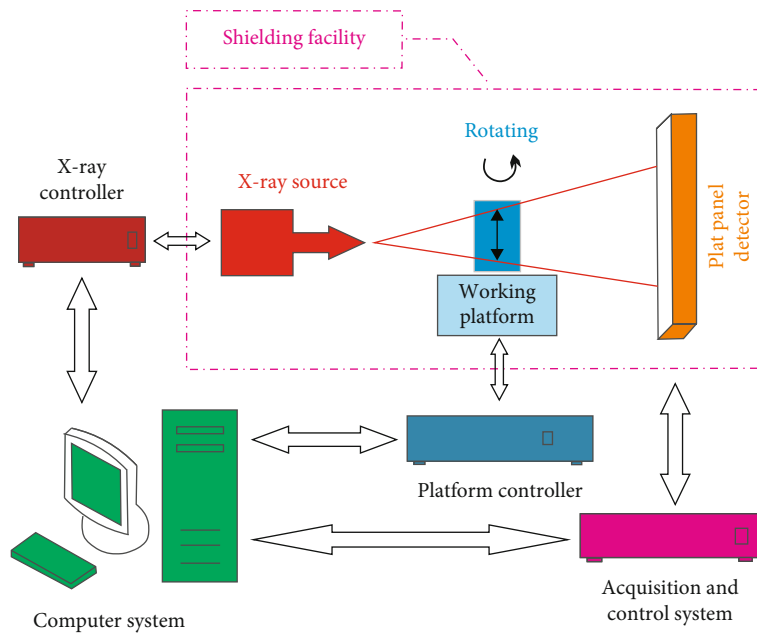

FIGURE 2: Schematic diagram of the industrial cone-beam X-ray system (modified after Ma [32]).

hydration and analyzed the relationships between damage variables and shale hydration under different stages based on the CT technique. Roshan et al. [9] performed a set of experiments on partially saturated shale samples and revealed that both capillary forces and surface-osmotic hydration control the water adsorption into partially saturated shale. Zhou et al. [10] qualitatively analyzed the effects of capillarity and osmosis diffusion on the imbibition process of shale. Liu et al. [11] researched the shale damage caused by hydration by immersion experiment and analyzed the mechanism of formation and propagation of cracks. Chakraborty et al. [12] presented an experimental study of water imbibition in shale and investigated the time-dependent permeability evolution. Zhang and Sheng [7] investigated the influence of hydration on permeability in shale, and generation fractures were observed by CT technique. The previous studies have clarified the effect of hydration on the internal structure of shale. However, how the remaining fracturing water affects the mechanical properties of shale formation is still not solved and needs further research.

In shale gas exploration, the remaining fracturing water and the production of shale gas will make the shale matrix shrink or swell, causing its strain. Thus, it is necessary to investigate the volumetric strain of shale induced by the combined effects of adsorption fluid and stress compression, especially the stress-volumetric strain curve, which is the sensitive indicator in the study of basic mechanical properties of shale [13, 14]. The earliest study that used the volumetric strain to analyze the deformation characteristics of rock was carried out by Brace et al. [15]. Later, many scholars have studied the volumetric strain characteristics of different rocks. For the sedimentary rocks, Jiang et al. [16], Hu et al. [17], and Lu and Liu [18] investigated the sandstone under uniaxial and triaxial compression tests. Gatelier et al. [19] researched the sandstone under two types of cyclic triaxial tests. Palchik and Hatzor [20] and Kelvis and Nordlund [21] analyzed the dolomite and limestone. Pellet and Fabre [22], He et al. [23], and Liang et al. [24] studied the argillaceous rocks, coal, and salt rocks, respectively. For the igneous rocks, Takarli et al. [25] and Liang et al. [26] analyzed the damage process of
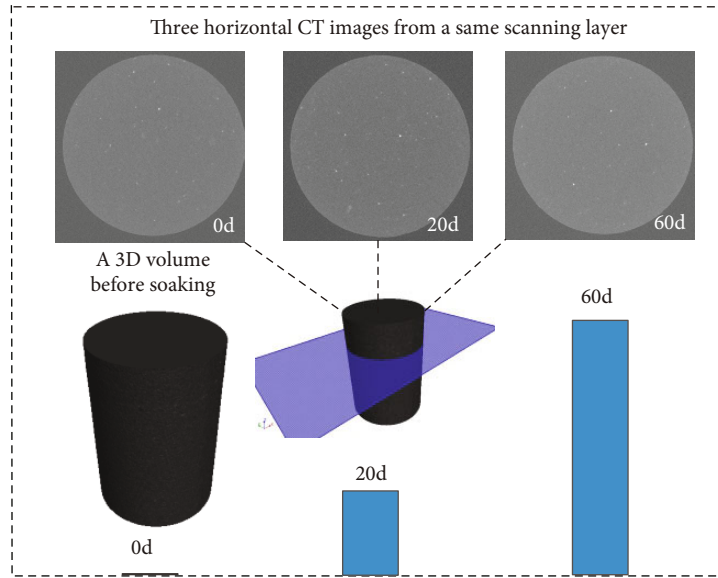
FIGURE 3: Scanning results of 3D volume before soaking and CT images after three hydration periods of S1.
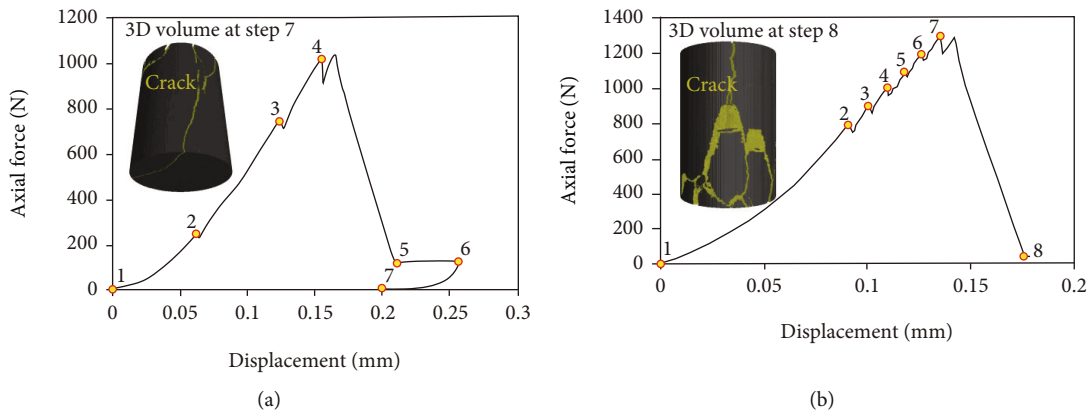

(a)

(b)

FIGURE 4: The axial force-displacement relationships and the reconstructed failure 3D volumes at the last scanning steps (the yellow areas are cracks) of S3 (a) and S4 (b).

granite. Pellet et al. [27] and Nicksiar and Martin [28] investigated the characteristics of gabbro and diorite, respectively. For the metamorphic rocks, Huang et al. [29] researched the stress-volumetric strain curves of marble at different loading strain rates. In all the experimental researches above, the deformation characteristics of rocks were described well using the volumetric strain. However, its value was calculated by using the directly measured axial strain and the lateral strain at a center portion of the tested specimen, which would cause the loss of information of the lateral strain in other locations and then the volumetric strain in the whole specimen.

To further study the water effect and the deformation characteristics of shale, some cylindrical specimens were soaked in water for a certain period of time, the in situ (loading and scanning at the same time) uniaxial compression tests were conducted, and the nondestructive CT technique was used for scanning at different hydration and loading stages. Based on the scanned CT results, the image gray variance value in each hydration specimen at different soaking

periods was extracted, and the evolution characteristics were quantitatively analyzed. The differences of the crack morphology after uniaxial compression tests between shale specimens with and without hydration process were also analyzed. In addition, a new method based on the CT images was proposed to calculate the lateral strain, and the evolution of axial stress-strain (including the axial strain, lateral strain, and volumetric strain) curve was revealed. At last, the differences of the expansion/compression degree along with specimen height were discussed.

2. Tested Specimens and Equipment

All prepared specimens were cored from the same shale block, which was taken from the outcrop shale formation in Shizhu, Chongqing, China (Figure 1(a)). During the indoor sample preparation, this shale block was fixed under the drill bit of a hand-operated electric drill, and shale specimens with horizontal bedding planes were prepared
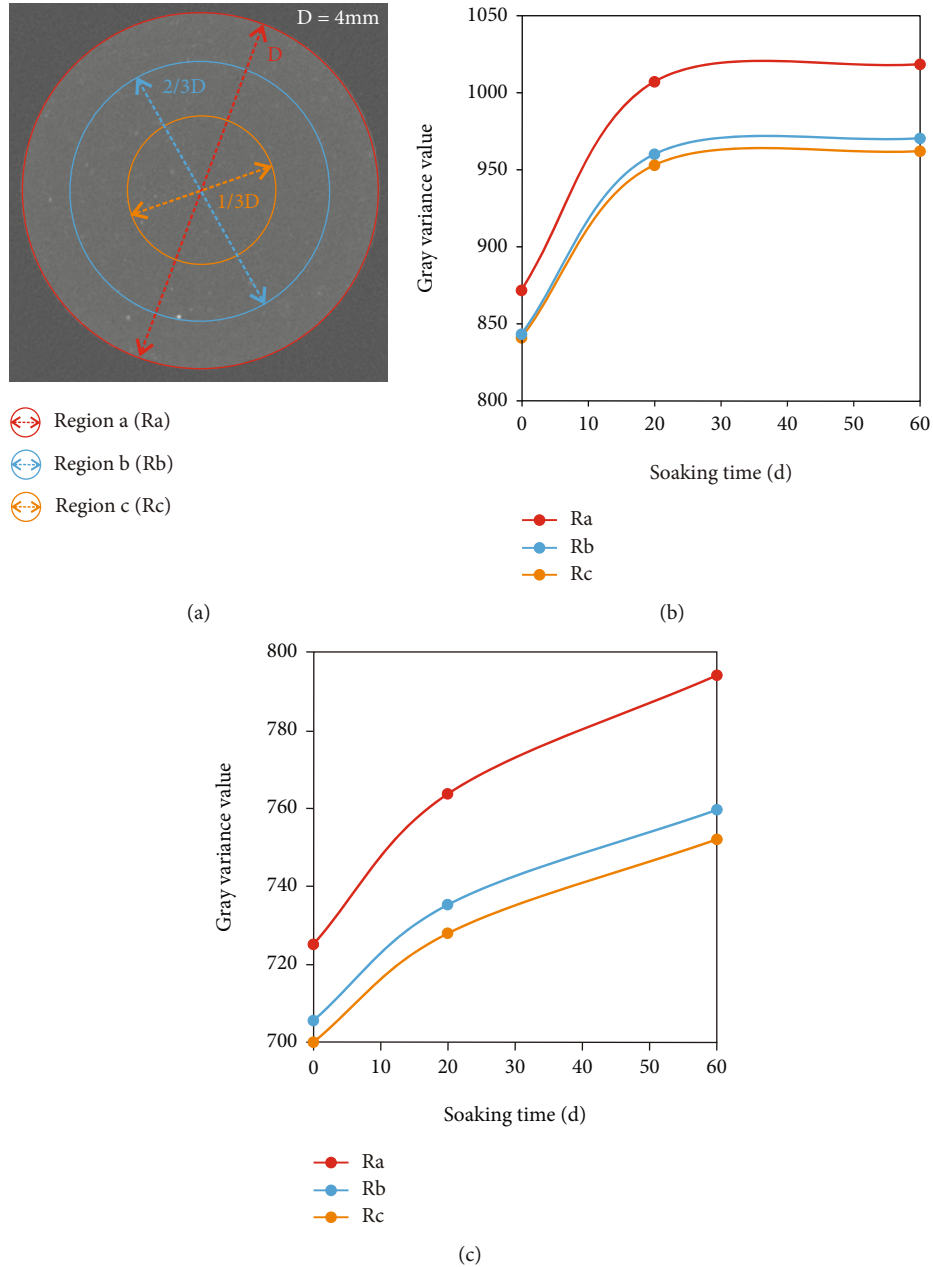
(a)

(b)

(c)

Figure 5: Diagram of statistical regions (a) and evolution curves of gray variance value in S1 (b) and S2 (c).

(Figure 1(b)). In order to obtain the parallel surfaces of samples for testing, a cutting-grinding machine was used to smooth the top and bottom of the drilling specimens. The size of each prepared specimen is with a diameter of 4 mm and a height of 8 mm (Figure 1(b)), and four specimens named S1, S2, S3, and S4 were prepared.

The micro-CT equipment available at the Institute of Geology and Geophysics, Chinese Academy of Sciences, Beijing, China, was used to scan the tested specimens' internal structures [30, 31]. Figure 2 shows the diagram of this device (ZEISS Xradia 520 Versa X-ray microscopy), which is mainly composed of an X-ray source (90 kV in voltage and 88.9 μA in current), working platform, X-ray detector (plat panel), mechanical scanning control system, and shielding facility. At each scanning step, the key workflows to obtain CT images include the following: (1) the X-ray source uses the cone-beam (cone angle of 5.11°), a full vertical projection can first be recorded on the detector after the X-ray had passed through the specimen; (2) the working platform was rotated with an angle of 0.2°, and the specimen was scanned again; (3) the rotating and scanning operations were repeated until the specimen completed a 360° rotating; and (4) those vertical projections were reconstructed to a three-dimensional (3D) volume, and then, the two-dimensional CT images in different directions can be segmented from 3D volume. In addition, for realizing the in situ uniaxial compression tests, a special loading apparatus (DEBEN Microtest CT5000) named the uniaxial
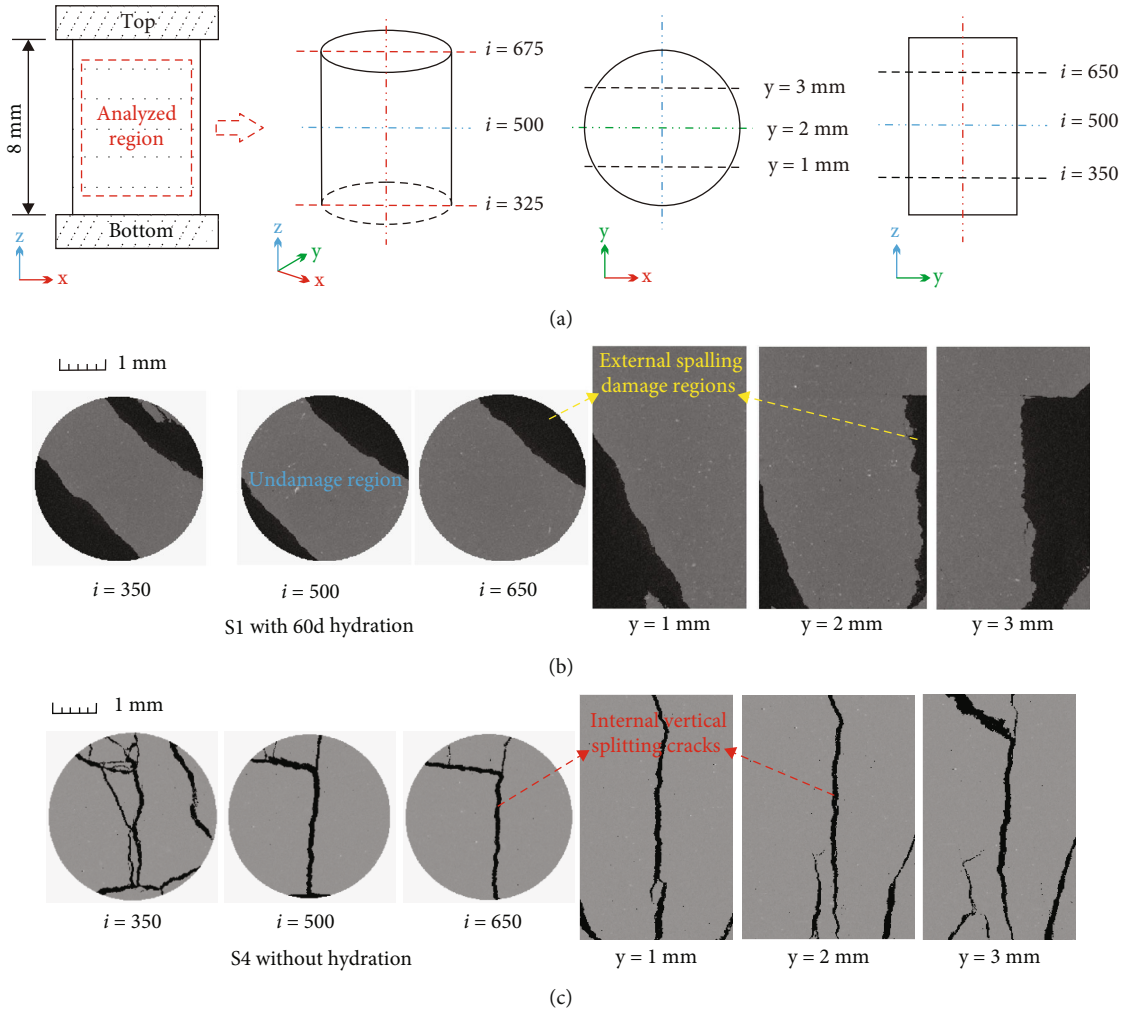
(a)

(b)

(c)

FIGURE 6: CT slice position (a) and results of failure S1 with 60d hydration (b) and S4 without hydration (c).

compression-tensile attachment was placed on the working platform, and the specimen can be scanned during loading. The maximum allowable pressure of this apparatus is 5 kN, the compression range is from 15 mm to 5 mm, and the adjustable displacement loading rate is 0.03-3 mm/min.

3. Experimental Process and Results

The prepared specimens, S1 and S2, were used for the hydration tests. Firstly, to obtain the internal structural characteristics of shale before soaking, the two specimens were scanned under the natural state using the high-resolution micro-CT equipment. Then, to compare the internal variation of shale after different water imbibition periods, some soaking tests and corresponding CT scanning tests were conducted. Each experimental specimen was first soaked into clean water at natural temperature (~20°C) and atmospheric pressure to begin the hydration. Then, the specimen was scanned after soaking for twenty days. After that, the specimen was put back into the water to continue the hydration for forty days, and then, the CT scanning operation was repeated after the hydration. Thus, the duration of a whole hydration experiment is

sixty days and the three periods of CT scanning are 0, 20, and 60 days. The hydration process and results of one of the specimens are shown in Figure 3. The 3D volume is the reconstructed result of the specimen before soaking. The horizontal CT images are the scanning results from the same elevation of S1 after three hydration periods.

The uniaxial compression tests at the minimal constant displacement rate of 0.03 mm/min were conducted in the prepared specimens, S3 and S4 without hydration and the tested S1 with hydration. Meanwhile, some in situ CT scans were completed at some force levels during loading, which means that the loading was stopped at some given stress values, and the CT scanning was performed. Figure 4 shows the loading curves (the axial force-displacement relationships) and the CT scanning steps (the yellow points, each one indicates the scanning step i) of S3 and S4. The CT scans of S3 were mainly distributed near the characteristic stress points (the yellow points in Figure 4(a)), and the CT scans of S4 mainly appeared around the peak strength (the yellow points in Figure 4(b)). At each scanning step, a 3D volume of the loading specimen can be reconstructed, and then, some horizontal CT images (named as i^{th} layer from bottom to top successively) can be obtained [33, 34].
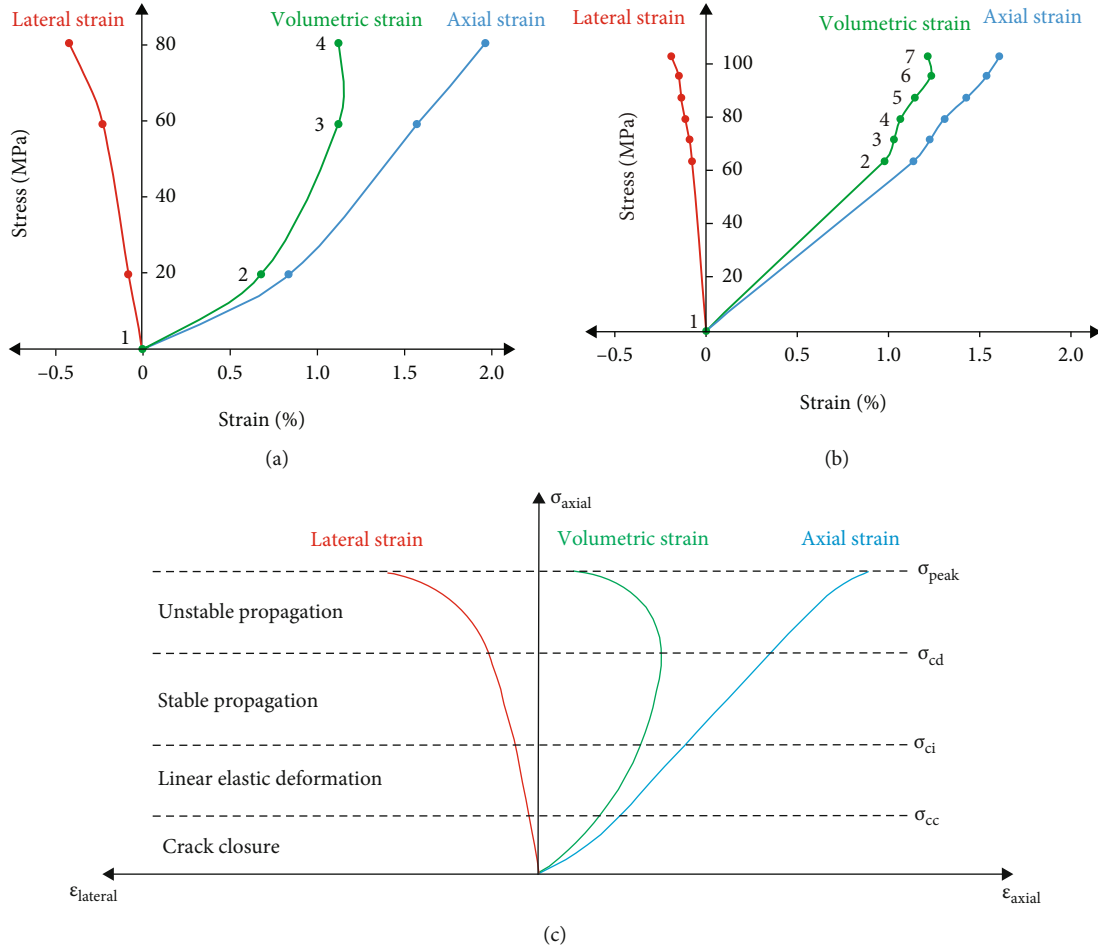
(a)

(b)

(c)

FIGURE 7: Uniaxial compression stress-strain curves of S3 (a), S4 (b), and Eberhardt et al. [40] (c).

4. Analysis of Hydration and Deformation Characteristics

4.1. Hydration Characteristics. In theory, a CT image is a digital image matrix, and the value of each pixel is presented by using the pixel gray level. The CT gray variance value of the collection points means the distance to the average value, which can reflect the density distribution characteristic of the internal structure of the scanned specimen from a CT image, and it can be used to quantitatively describe the difference of internal structures [35, 36]. Thereafter, based on the CT images scanned at three soaking periods, the CT gray variance values in S1 and S2 were extracted using the Mimics Research software. For the results of each scanning, some horizontal CT images from the center layers ($i^{th} = 325^{th}$ to 675th) were chosen for statistics, and for each image, there are three statistical regions A, B, and C (Ra, Rb, and Rc) were selected, as shown in Figure 5(a), the three regions are three concentric circles, and the diameters of them are equal to the specimen diameter (D, where $D = 4$ mm), two-thirds diameter (2/3 D), and one-third diameter (1/3 D).

The CT gray variance value of each statistical region at different layers can be obtained, and then, the average value can be calculated. The results of S1 and S2 are shown in Figures 5(b) and 5(c), respectively. The evolution curves

reveal that the gray variance values of S1 and S2 show an increasing trend in the process of soaking. The growth trend is almost the same at different statistical regions (Ra, Rb, and Rc) of each specimen, and the values in Ra (the red points and curves) are the largest in both specimens. Those indicate that the water soaking can change the structural characteristics of shale, and the influence degree is more evident in the outer region than the internal region. Moreover, it was found that in the early stage of soaking (0-20d), the image gray variance values in the three statistical regions of S1 and S2 both increased rapidly, which indicates that water has a significant influence on the internal structure of shale in the early stage of soaking. In the later stage of soaking (20-60d), each statistical region's image gray variance curves in S1 gradually slowed down. In contrast, the three curves in S2 still showed a rapid rise, indicating that the water influence on S1 tended to be stable, and the effect on S2 continued.

4.2. Hydration Effect. As mentioned above, water soaking with different periods influences the evolution of the internal structure of shale. To further study the effect of water soaking on the mechanical property of shale, the S1 with 60d water imbibition was also subjected to a uniaxial compression test, and the failure specimen was observed using the micro-CT equipment. Then, the influence of hydration on
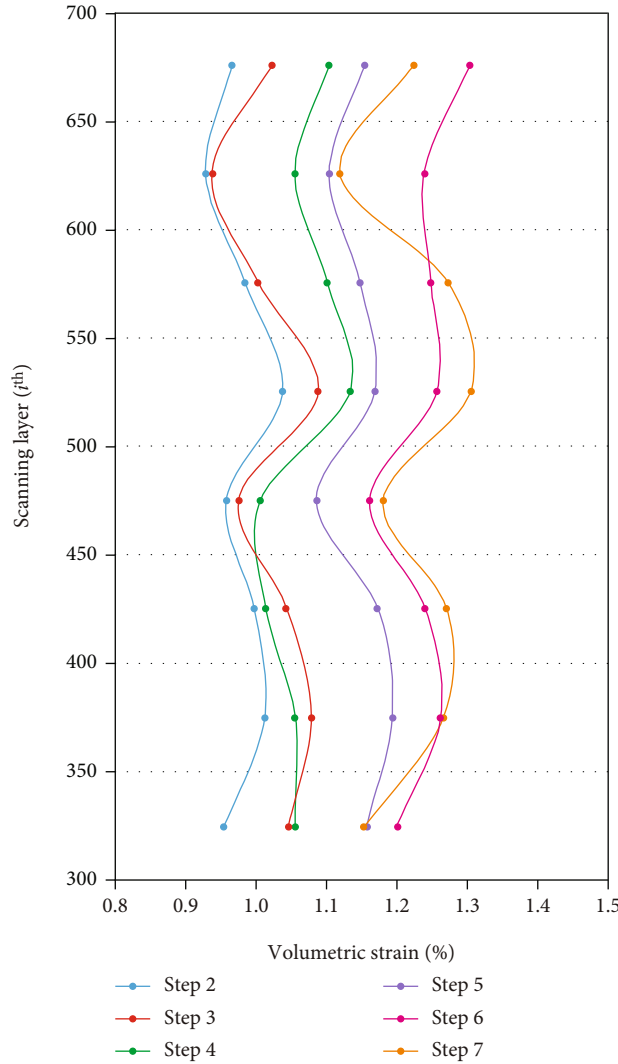
FIGURE 8: Volumetric strain distributions along with specimen height at different scanning steps for S4.

shale fracturing characteristics was analyzed by comparing the internal crack distribution of specimens with hydration and without hydration. Figure 6(a) shows the diagram of CT slice position for a 3D reconstructed CT volume, there are three horizontal CT slices ($i^{th} = 350^{th}$, 500th, and 650th) and three vertical CT slices ($y = 1$ mm, 2 mm, and 3 mm) of each specimen is selected. Figures 6(b) and 6(c) give the scanning results of failure S1 with 60d water imbibition and S4 without water imbibition.

It was found that the failure regions were distributed mainly in the external position of S1 from Figure 6(b) according to the basic principle of X-ray CT [31, 37]. The CT results show that the failure of the specimen is primarily the whole piece spalling in the outer region after the uniaxial compression test. Those phenomena indicate that the hydration degree in the peripheral area was high. It was consistent with the characterization results of gray variance (Figure 5), and it resulted in the crack morphology that the external spalling damage regions were dominant. In addition, the failure characteristics of S1 with hydration were compared

with that of S4 without hydration. It was found that the outer area of S1 was severely damaged, and the damaged part presented as some whole irregular blocks (Figure 6(b)), and some vertical splitting cracks occurred in the internal position of S4 (Figure 6(c)) after the uniaxial compression test destroyed them. Those differences in the crack morphology indicate that the hydration treatment affects the failure mode of the specimen, especially the outer regions of shale.

4.3. Deformation Characteristics. As mentioned above, the deformation characteristics of rocks can be described quantitatively using the volumetric strain. In theory, the changing of the specimen volumes (the volumetric strain) can be directly calculated after obtaining the 3D reconstructed stereograms at some force levels during the loading process. However, to eliminate the influence of the end-effect, some CT images from the center layers ($i^{th} = 325^{th}$ to 675th) of specimens at each scanning step were chosen to analyze the deformation characteristics. The specific method and results are as follows.

(a)   (b)
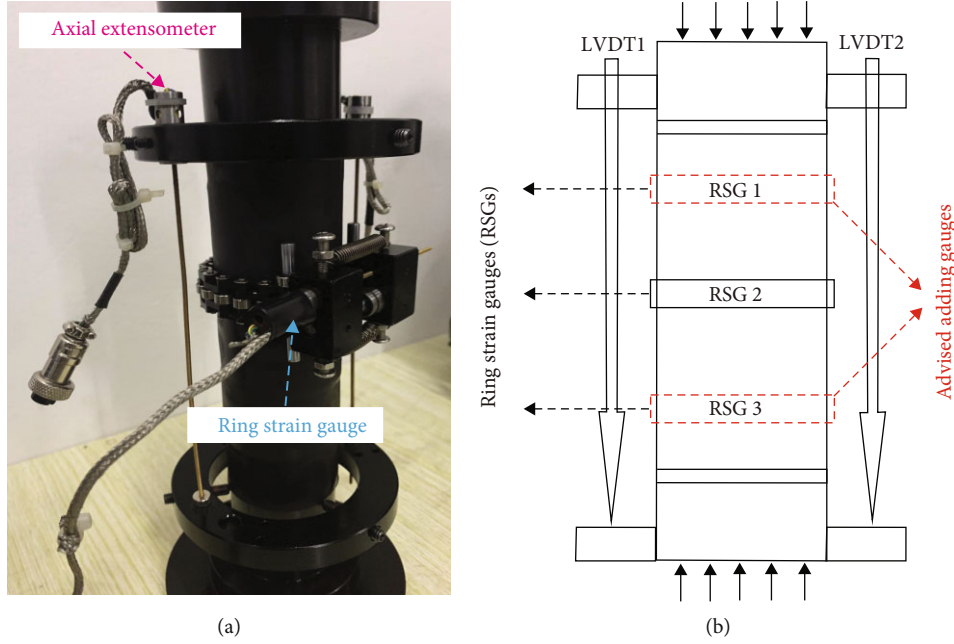
FIGURE 9: The measuring method of the lateral strain before (a) and after (b) advised.

4.3.1. Calculating Method. According to the definition of elastic mechanics [31, 38], when compression is positive, the volumetric strain is defined as

$$\varepsilon_v = \frac{-(V - V_0)}{V_0} = \frac{-\Delta V}{V_0}. \tag{1}$$

For a cylindrical specimen, the formula is expressed as

$$\varepsilon_v = \frac{-\Delta V}{V_0} = \varepsilon_y + 2\varepsilon_x, \tag{2}$$

where V_0 and V are the specimen volumes before and after the deformation of rocks, ε_v, ε_x, and ε_y are the volumetric strain, lateral strain, and axial strain of a cylindrical specimen, respectively.

In the in situ uniaxial compression tests, the axial strain was calculated from the changing of the measuring displacement during loading. The lateral strain was not measured during testing, but it was calculated using a new method based on CT image, which is expressed as

$$\varepsilon_x = -\frac{(P_i - P_0)}{P_0}, \tag{3}$$

where P_0 is the perimeter of rock specimen before loading and P_i is the perimeter after loading to the scanning step i.

For each scanning specimen, a scanning layer corresponds to a value of perimeter. The specimen perimeters in CT images at different layers and scanning steps can be measured using the Image-Pro-Plus (IPP) software. Thus, the statistical perimeters from the same layer at different scanning steps can be plugged into Equation (3) successively, the lateral strain at different layers can be calculated; then,

the lateral results and the calculated axial strain can be plugged into Equation (2), the volumetric strain along with the specimen height can be obtained.

4.3.2. Calculation Results. An average value of the volumetric strain from different scanning layers can be calculated considering the statistical height. Figure 7 shows the stress-strain curves (including the axial strain, lateral strain, and volumetric strain) before peak strength of the two specimens under in situ uniaxial compression conditions. For S3 (Figure 7(a)), although the axial strain curve changes almost in linear, the volumetric strain curve begins to deviate from linearity almost from scanning step 2, which means that the microcracks inside the rock are further developed, or the pore spaces are further deformed. From scanning step 3 to step 4, the deviation degree of the volumetric curve is even worse, and the back-bending phenomenon can be observed, which indicates the beginning of the crack instability expansion, and this corresponds to the phenomenon that there are existing cracks at step 3 from CT images [39]. For S4 (Figure 7(b)), although there are no obvious cracks existed in CT images before peak strength, the stress-volumetric strain curve has slightly deviated from linearity, which indicates the formation and the development of the internal microcracks. The evolution law of those stress-strain curves in this study corresponds to the result of Eberhardt et al. [40], which divided the evolution process into four stages (the crack closure, linear elastic deformation, stable propagation, and unstable propagation stages) according to the characteristics of stress-strain curves (Figure 7(c)). Here, the evolution stages in both in situ testing shale specimens are not specifically divided, but the expansion phenomena before compressive strength are indeed observed, and the overall trends are both consistent with the previous research.

5. Discussion

The average volumetric strain can reflect the evolution characteristics of deformation in the whole specimen, but it cannot reflect the deformation differences along with the specimen height. Figure 8 shows the volumetric strain distributions along with the specimen height at different scanning steps of S4. In the first six scanning steps, it is obvious that the values of the volumetric strain in the whole height direction all increase with the scanning steps, which indicates that the S4 was almost compressed. At the seventh scanning step, values of the volumetric strain at the top and bottom parts have a rebound, and the degree of enlargement in the middle part has decreased, which means the formation and development of damage from both ends. Additionally, it was found that the stain curve at each step looks like an upright sine curve, which indicates the different degrees of compression along with the specimen height and may be caused by the existence of the horizontal bedding planes of shale. Due to the differences in physical properties, the bedding plane's position is more easily deformed than the matrix's position, leading to an upright sine curve of volumetric strain and indicating the compression differences along with the specimen height.

From the volumetric strain results at different scanning layers and steps, the differences of the expansion or compression degrees along with the specimen height were observed, and the development of the internal damage along with the specimen height was reflected correspondingly. Those deformation differences cannot be obtained from the conventional rock mechanics tests, because the lateral strain was measured only in the middle position using the resistance strain gauge or the ring strain gauge (Figure 9 (a)). Thus, to obtain the strain characteristics along with the specimen height in laboratory tests, an improved measuring method of strain was advised. Another two groups of strain gauges can be used in positions at one-quarter height and three-quarters height of the specimen (Figure 9 (b)), considering the size of the strain gauge and the standard rock specimen. If the size of the rock specimen allowed more strain gauges to be installed, the numbers of the lateral strain gauges could be added accordingly. For the conventional tests, this advised method can resolve the measuring of the strain differences along with the specimen height easily by adding the standard strain equipment and does not cost much.

6. Conclusions

To further obtain the water effect and the deformation characteristics of shale, the cylindrical specimens were soaked in water for three periods, the uniaxial compression tests were conducted, and the CT technique was used for scanning at different hydration and loading stages. Based on the CT results, the evolution characteristics of image gray variance value in each hydration specimen and the differences of the hydration effect on failure characteristics were quantitatively analyzed. In addition, the evolution of axial stress-volumetric strain curves based on a new method was revealed, and the deformation degree along with the specimen height was discussed. The conclusions drawn from this study are as follows:

(1) The hydration specimens were scanned at three soaking periods of 0, 20, and 60 days, and the CT gray variance values at three soaking periods and three statistical regions of each specimen were analyzed. The evolution results show that the water imbibition can change the internal structure of shale, and it has a significant influence in the early stage of soaking. The influence degree is more evident in the external region in the entire soaking period

(2) The water influence on shale mechanical property was analyzed by comparing the failure characteristics of specimens with and without hydration. The CT results show that the outer part of the specimen with hydration was severely damaged, and some vertical splitting cracks occurred in the internal position of the specimen without hydration. Those differences indicate that the hydration treatment affects the failure mode of shale

(3) A new method based on the perimeter changing of specimens in CT image was proposed to calculate the lateral strain and the volumetric strain. The morphologies of stress-strain curves (including the axial strain, lateral strain, and volumetric strain) before peak strength show that the expansion phenomena exist before failure, and the overall evolution law is consistent with the previous research that divided the evolution process into four stages

(4) The values of volumetric strain from CT image at different scanning layers were discussed in detail, and the results reflect the differences in the expansion or compression degree along with the specimen height. To measure the strain differences along with the specimen height as more as possible, an improved measuring method of the lateral strain was advised by adding another two groups (or more) strain gauges in the conventional experiments

Data Availability

The data used to support the findings of this study are included within the article.

Conflicts of Interest

The authors declare no conflict of interest.

Acknowledgments

References

[1] C. L. Ya, J. G. Deng, Y. F. Cheng, M. L. Li, Y. C. Feng, and X. R. Li, "Mechanical properties of gas shale during drilling operations," *Rock Mechanics and Rock Engineering*, vol. 50, no. 7, pp. 1753–1765, 2017.

[2] Z. J. Jin, Z. R. Bai, B. Gao, and M. W. Li, "Has China ushered in the shale oil and gas revolution?," *Oil and Gas Geology*, vol. 40, no. 3, pp. 451–458, 2019.

[3] J. Wang, Y. Wang, S. Li, and L. Yang, "Strength softening characteristics of shale clay mineral expansion," *Chemistry and Technology of Fuels and Oils*, vol. 56, no. 2, pp. 300–311, 2020.

[4] L. C. Jia, M. Chen, L. T. Sun et al., "Experimental study on propagation of hydraulic fracture in volcanic rocks using industrial CT technology," *Petroleum Exploration and Development*, vol. 40, no. 3, pp. 405–408, 2013.

[5] B. Hou, R. X. Zhang, Y. J. Zeng, W. N. Fu, Y. F. Muhadasi, and M. Chen, "Analysis of hydraulic fracture initiation and propagation in deep shale formation with high horizontal stress difference," *Journal of Petroleum Science and Engineering*, vol. 170, pp. 231–243, 2018.

[6] H. Singh, "A critical review of water uptake by shales," *Journal of Natural Gas Science and Engineering*, vol. 34, no. 2, pp. 751–766, 2016.

[7] S. F. Zhang and J. J. Sheng, "Effect of water imbibition on fracture generation in Mancos shale under isotropic and anisotropic stress conditions," *Journal of Geotechnical and Geoenvironmental Engineering*, vol. 144, no. 2, article 04017113, 2018.

[8] T. S. Ma and P. Chen, "Study of meso-damage characteristics of shale hydration based on CT scanning technology," *Petroleum Exploration and Development*, vol. 41, no. 2, pp. 249–256, 2014.

[9] H. Roshan, S. Ehsani, C. E. Marjo, M. S. Andersen, and R. I. Acworth, "Mechanisms of water adsorption into partially saturated fractured shales: an experimental study," *Fuel*, vol. 159, pp. 628–637, 2015.

[10] Z. Zhou, H. Abass, X. Li, D. Bearinger, and W. Frank, "Mechanisms of imbibition during hydraulic fracturing in shale formations," *Journal of Petroleum Science and Engineering*, vol. 141, pp. 125–132, 2016.

[11] X. J. Liu, W. Zeng, L. X. Liang, and J. Xiong, "Experimental study on hydration damage mechanism of shale from the Longmaxi Formation in southern Sichuan Basin, China," *Petroleum*, vol. 2, no. 1, pp. 54–60, 2016.

[12] N. Chakraborty, Z. T. Karpyn, S. Liu, and H. Yoon, "Permeability evolution of shale during spontaneous imbibition," *Journal of Natural Gas Science and Engineering*, vol. 38, pp. 590–596, 2017.

[13] S. L. Crouch, "Experimental determination of volumetric strains in failed rock," *International Journal of Rock Mechanics and Mining Sciences*, vol. 7, no. 6, pp. 589–603, 1970.

[14] W. Tian and H. Q. Liu, "Insight into the adsorption of methane on gas shales and the induced shale swelling," *American Chemical Society*, vol. 5, pp. 31508–31517, 2020.

[15] W. F. Brace, B. W. Paulding Jr., and C. Scholz, "Dilatancy in the fracture of crystalline rocks," *Journal of Geophysical Research*, vol. 71, no. 16, pp. 3939–3953, 1966.

[16] Y. D. Jiang, X. F. Xian, D. G. Xiong, and F. C. Zhou, "Study on creep behaviour of sandstone and its mechanical models," *Chinese Journal of Geotechnical Engineering*, vol. 27, no. 12, pp. 1479–1481, 2005.

[17] D. W. Hu, H. Zhou, F. Zhang, and J. F. Shao, "Evolution of poroelastic properties and permeability in damaged sandstone," *International Journal of Rock Mechanics and Mining Sciences*, vol. 47, no. 6, pp. 962–973, 2010.

[18] X. L. Lu and Q. S. Liu, "Experimental investigation of dilatancy-bulking behavior of weak sandstone," *Advanced Materials Research*, vol. 197-198, pp. 1420–1424, 2011.

[19] N. Gatelier, F. Pellet, and B. Loret, "Mechanical damage of an anisotropic porous rock in cyclic triaxial tests," *International Journal of Rock Mechanics and Mining Sciences*, vol. 39, no. 3, pp. 335–354, 2002.

[20] V. Palchik and Y. H. Hatzor, "Crack damage stress as a composite function of porosity and elastic matrix stiffness in dolomites and limestones," *Engineering Geology*, vol. 63, no. 3-4, pp. 233–245, 2002.

[21] P. H. Kelvis and E. Nordlund, "Comparison between stress and strain quantities of the failure-deformation process of Fennoscandian hard rocks using geological information," *Rock Mechanics and Rock Engineering*, vol. 46, no. 1, pp. 41–51, 2013.

[22] F. L. Pellet and G. Fabre, "Damage evaluation with p-wave velocity measurements during uniaxial compression tests on argillaceous rocks," *International Journal of Geomechanics*, vol. 7, no. 6, pp. 431–436, 2007.

[23] M. C. He, C. G. Wang, J. L. Feng, D. J. Li, and G. Y. Zhang, "Experimental investigations on gas desorption and transport in stressed coal under isothermal conditions," *International Journal of Coal Geology*, vol. 83, no. 4, pp. 377–386, 2010.

[24] W. G. Liang, Y. S. Zhao, S. G. Xu, and M. B. Dusseault, "Effect of strain rate on the mechanical properties of salt rock," *International Journal of Rock Mechanics and Mining Sciences*, vol. 48, no. 1, pp. 161–167, 2011.

[25] M. Takarli, W. Prince, and R. Siddique, "Damage in granite under heating/cooling cycles and water freeze-thaw condition," *International Journal of Rock Mechanics and Mining Sciences*, vol. 45, no. 7, pp. 1164–1175, 2008.

[26] C. Y. Liang, X. Li, S. X. Wang, S. D. Li, J. M. He, and C. F. Ma, "Experimental investigations on rate-dependent stress-strain characteristics and energy mechanism of rock under uniaxial compression," *Chinese Journal of Rock Mechanics and Engineering*, vol. 31, no. 3, pp. 1830–1838, 2012.

[27] F. L. Pellet, M. Keshavarz, and K. Amini-Hosseini, "Mechanical damage of a crystalline rock having experienced ultra high deviatoric stress up to 1.7 GPa," *International Journal of Rock Mechanics and Mining Sciences*, vol. 48, no. 8, pp. 1364–1368, 2011.

[28] M. Nicksiar and C. D. Martin, "Evaluation of methods for determining crack initiation in compression tests on low-porosity rocks," *Rock Mechanics and Rock Engineering*, vol. 45, no. 4, pp. 607–617, 2012.

[29] D. Huang, R. Q. Huang, and Y. X. Zhang, "Experimental investigations on static loading rate effects on mechnical properties and energy mechanism of coarse crystal grain marble under uniaxial compression," *Chinese Journal of Rock Mechanics and Engineering*, vol. 31, no. 2, pp. 245–255, 2012.

[30] B. C. Yang, L. Xue, Y. T. Duan, and M. M. Wang, "Correlation study between fracability and brittleness of shale-gas reservoir," *Geomechanics and Geophysics for Geo-Energy and Geo-Resources*, vol. 7, no. 2, p. 31, 2021.

[31] Y. T. Duan and B. C. Yang, "How does structure affect the evolution of cracking and the failure mode of anisotropic shale?," *Geomechanics and Geophysics for Geo-Energy and Geo-Resources*, vol. 8, no. 1, p. 25, 2022.

[32] J. F. Ma, *Research of 3D cone-beam CT image reconstruction accelerating technology*, Shandong University Master's Thesis, 2011.

[33] Y. T. Duan, X. Li, P. G. Ranjith, and Y. F. Wu, "An investigation of the evolution of the internal structures and failure modes of Longmaxi shale using novel X-ray microscopy," *Journal of Petroleum Science and Engineering*, vol. 184, article 106479, 2020.

[34] B. C. Yang, S. Q. Qin, L. Xue, and H. R. Chen, "The reasonable range limit of the shape parameter in the Weibull distribution for describing the brittle failure behavior of rocks," *Rock Mechanics and Rock Engineering*, vol. 50, no. 6, pp. 3359–3367, 2021.

[35] Y. T. Duan, X. Li, B. Zheng, J. M. He, and J. Hao, "Cracking evolution and failure characteristics of Longmaxi shale under uniaxial compression using real-time computed tomography scanning," *Rock Mechanics and Rock Engineering*, vol. 52, no. 9, pp. 3003–3015, 2019.

[36] Y. T. Duan, X. Li, J. M. He, S. D. Li, and R. Q. Zhou, "Quantitative analysis of meso-damage evolution for shale under in situ uniaxial compression conditions," *Environmental Earth Sciences*, vol. 77, no. 4, pp. 154–162, 2018.

[37] Y. Wang, H. N. Yang, J. Q. Han, and G. Zhu, "Effect of rock bridge length on fracture and damage modelling in granite containing hole and fissures under cyclic uniaxial increasing-amplitude decreasing-frequency (CUIADF) loads," *International Journal of Fatigue*, vol. 158, p. 106741, 2022.

[38] L. Y. Li, H. P. Xie, X. Ma, Y. Ju, T. W. Tang, and Q. J. Fang, "Experimental study on relationship between surface temperature and volumetric strain of rock under uniaxial compression," *Journal of China Coal Society*, vol. 37, no. 9, pp. 1511–1515, 2012.

[39] X. Li, Y. T. Duan, S. D. Li, and R. Q. Zhou, "Study on the progressive failure characteristics of Longmaxi shale under uniaxial compression conditions by X-ray micro-computed tomography," *Energies*, vol. 10, no. 3, p. 303, 2017.

[40] E. Eberhardt, D. Stead, B. Stimpson, and R. S. Read, "Identifying crack initiation and propagation thresholds in brittle rock," *Canadian Geotechnical Journal*, vol. 35, no. 2, pp. 222–233, 1998.